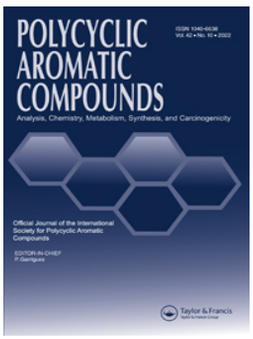

Polycyclic Aromatic Compounds

ISSN: (Print) (Online) Journal homepage: https://www.tandfonline.com/loi/gpol20

Structural, Quantum Chemical, Molecular Docking, and Dynamics Studies of Quercetin—A Potent Inhibitor for Colon Cancer

Abraham Hudson Mark J., Premkumar R., Sangeetha R., Lakshmi A. & Langeswaran K.

To cite this article: Abraham Hudson Mark J., Premkumar R., Sangeetha R., Lakshmi A. & Langeswaran K. (2022): Structural, Quantum Chemical, Molecular Docking, and Dynamics Studies of Quercetin—A Potent Inhibitor for Colon Cancer, Polycyclic Aromatic Compounds, DOI: 10.1080/10406638.2022.2149574

To link to this article: https://doi.org/10.1080/10406638.2022.2149574

Published online: 30 Nov 2022.

POLYCYCLIC AROMATIC COMPOUNDS
https://doi.org/10.1080/10406638.2022.2149574

Taylor & Francis
Taylor & Francis Group

Structural, Quantum Chemical, Molecular Docking, and Dynamics Studies of Quercetin—A Potent Inhibitor for Colon Cancer

Abraham Hudson Mark J.[a], Premkumar R.[b], Sangeetha R.[c], Lakshmi A.[c], and Langeswaran K.[d]

[a]Department of Physics, SSM Institute of Engineering and Technology, Dindigul, India; [b]PG and Research Department of Physics, N.M.S.S.V.N. College, Madurai, India; [c]Department of Physics, Mannar Thirumalai Naicker College, Madurai, India; [d]Department of Biotechnology, Alagappa University, Science Campus, Karaikudi, India

ABSTRACT

According to several studies, phytochemicals, such as polyphenols, flavones, and flavonoids have significant anticancer properties that can combat various malignancies. Even though its action is highly dependent on the intracellular availability of reduced glutathione, Quercetin is regarded as an excellent free-radical scavenging antioxidant flavonoid. Apart from its antioxidant properties, Quercetin has a direct pro-apoptotic action in tumor cells. It has been shown to inhibit the proliferation of multiple human cancer cell lines at various cell cycle stages. The choice of a suitable chemopreventive agent was based on epidemiological studies that showed that consuming a specific dietary component (e.g. Quercetin) can lower the incidence of specific cancer death. MLK4 (KIAA1804) is the second most often altered kinase in colorectal carcinomas with microsatellite stability (MSS) (CRC). MLK4 regulates various physiological cellular processes, including cell cycle, senescence, and apoptosis, and mechanistic evidence suggests MLK4 is involved in carcinogenesis. In this study, the molecular structure of the Quercetin molecule was optimized using DFT/B3LYP method with a cc-pVTZ basis set, and the structural parameters were calculated. The generated vibrational spectra and the optimized molecular geometry were thoroughly reviewed and compared with experimental findings, resulting in a strong correlation. FMOs analysis was performed, which confirms the molecular reactivity of the Quercetin molecule. The anti-tumor efficacy of Quercetin was examined against the colon cancer target protein through in silico parameters, such as molecular docking and dynamics, ADME studies, MM-GBSA calculations, and the Pharmacophore hypothesis. From the analysis, the docked complex showed the highest docking score and maintained the complex stability and flexibility throughout the simulation period. Thus, the present study concluded that Quercetin could be a potent inhibitor of targeted colon cancer protein.

ARTICLE HISTORY
Received 19 September 2022
Accepted 12 November 2022

KEYWORDS
Quercetin; colon cancer; UV-Vis spectrum; molecular docking and dynamics; MM-GBSA

CONTACT Langeswaran K. dr.langeswaran@gmail.com Cancer Informatics Laboratory, Department of Biotechnology, Alagappa University, Science Campus, Karaikudi, 630 003, Tamil Nadu, India; Sangeetha R. drsangeethamtnc@gmail.com Department of Physics, Mannar Thirumalai Naicker College, Pasumalai, Madurai, Tamil Nadu, India

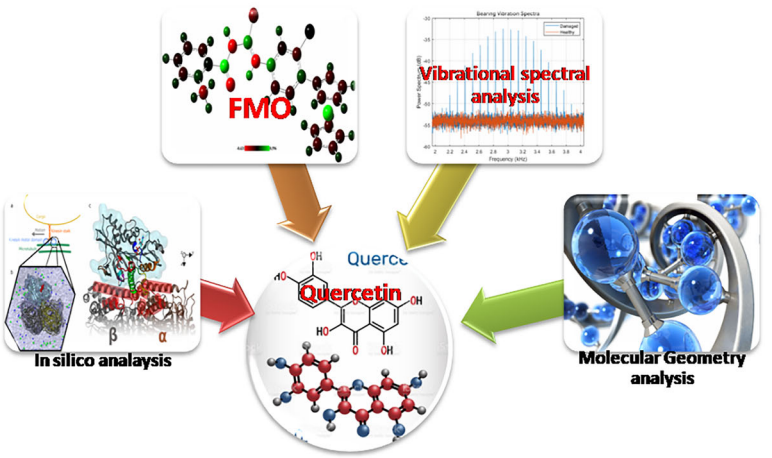

1. Introduction

Flavonoids are polyphenolic substances found in plants classified as flavonols, flavones, flavanones, isoflavones, catechins, anthocyanidins, and chalcones on their chemical structure. According to several studies, phytochemicals, such as polyphenols, flavones, and flavonoids have significant anticancer properties that can combat a variety of malignancies.[1] The antioxidant impact of this flavonoid is maybe its most essential feature. In addition, Quercetin may be beneficial in the prevention of cancer. The flavone molecule quercetin (3,3′,4′,5,7-pentahydroxyflavone) belongs to the flavonoids family.

It is abundant in the form of glycoside in a range of plants, fruits, and vegetables, such as onion, buckwheat, and broccoli, and is a natural product in the human diet. It's been added to functional foods as a commercial dietary supplement and has been shown to help prevent and treat illnesses like cancer.[2] Many naturally occurring substances, such as resveratrol1, 2-methoxyestradiol, luteolin derivatives, ellagic acid, and synthetic medicines used in chemotherapy, such as doxorubicin cisplatin, and others, have been combined with Quercetin. Combination treatment with Quercetin had synergistic results in several cases.[3] Flavonoids are the most researched anticancer and cancer-prevention medications.

Quercetin is a flavonoid with high potential in oncology due to its chemopreventive effects evidenced *in vitro* and *in vivo* models. Quercetin elicits biphasic, dose-dependent effects. At low concentrations, Quercetin acts as an antioxidant, and thus elicits chemopreventive effects, but at high concentrations, Quercetin functions as a pro-oxidant and may, therefore, elicit chemotherapeutic effects. Quercetin's anticancer effects rely on its ability to reduce proliferation, induce apoptosis, cause cell cycle arrest and inhibit mitotic processes by modulating cyclins, pro-apoptotic, PI3K/Akt, and mitogen-activated protein kinase (MAPK) molecular pathways. These chemicals can interfere with particular phases of the carcinogenic process, decrease cell growth, and cause apoptosis in various cancer cells. Colon cancer is typical cancer with a high mortality and morbidity rate worldwide. To determine the Quercetin compound's characteristics, such as metal-ligand bond strengths, binding energies, transition barriers, and relative conformational energies. To determine the extent to which its prediction may be relied on, DFT must be calibrated.[4] MLKs are a group of serine-threonine kinases that are considered to regulate a variety of intracellular signaling pathways. MLKs have an SRC-homology domain at the amino terminus, a kinase domain, a leucine-zipper region, and a Cdc42/Rac-interactive binding (CRIB) motif. Although all MLKs have a proline-rich carboxyl terminus, it differs significantly amongst family members, indicating that this region has various regulatory roles.[5]

The electronic structure of atoms, molecules, and solids can be calculated using density functional theory (DFT), a quantum-mechanical (QM) technique. Chemical reaction mechanisms, structural and spectroscopic characteristics, and other concerns are all elucidated using DFT, frequently with high dependability. DFT helps to determine an atom, molecule, or solid electronic structure in physics and chemistry. The molecular docking approach can mimic the interaction between a small molecule and a protein at the atomic level, allowing us to characterize the behavior of small molecules in the binding sites of target proteins and illuminate fundamental biochemical processes. Through docking, it is possible to find new drugs with therapeutic potential, predict molecular interactions between ligands and targets, and much more. Molecular dynamics simulations, a sophisticated technique, can now effectively understand the relationships between macromolecular structure and function. The simulation process time is quite close to a biologically important phase. By using the information on the dynamic characteristics of macromolecules, it is feasible to shift the traditional paradigm of structural bioinformatics from studying single structures to analyzing conformational ensembles.

In the present study, the molecular structure of the Quercetin molecule was optimized, and the vibrational frequencies were calculated. The calculated vibrational wavenumbers were assigned based on potential energy distribution calculations and compared with the reported experimental wavenumbers. Frontier molecular orbitals (FMOs) analysis was used to determine the molecule's chemical hardness, potential, and electronegativity. The UV-Visible spectrum of the Quercetin molecule was simulated in gas and ethanol phases. Molecular electrostatic potential (MEP) surface and Mulliken atomic charge distribution analysis were also carried out to confirm the reactive nature of the molecule. In addition to that, the anti-cancerous efficacy of the Quercetin molecule was examined against colon cancer target receptors through computational approaches, including molecular docking, ADME studies, pharmacophore modeling, and molecular dynamics simulation.

2. Methodology

2.1. Quantum chemical calculations

Quercetin (Compound ID: 5280343) molecule was optimized using the DFT/B3LYP method with cc-pVTZ basis set using Gaussian 09 program.[6] The vibrational wavenumbers of the molecule were calculated and assigned based on PED calculations using the VEDA 4.0 programme.[7] The Gauss View 05 visualization tool displayed the investigated molecule's molecular structure, FMOs, and molecular electrostatic potential (MEP) surface. Mulliken atomic charge values of the Quercetin molecule were calculated using Mulliken population analysis. All DFT calculations were performed at the ground state energy level of the Quercetin molecule, with no constraints on the potential energy surface.

2.2. Target identification and preparation

The target receptor was downloaded from the PDB (Protein Data Bank) database.

The following approaches were performed; a protein preparation panel was used to prepare the target receptor. The target bound with the co-crystallized water molecules, which were deleted and refined the structure by optimizing and minimizing using the force field OPLS_2005.[8] In this present study, MLK4 kinase protein was the targeted receptor molecule. MLK4 (KIAA1804) is the second most often altered kinase in colorectal carcinomas with microsatellite stability (MSS). The mechanistic study evidenced that MLK4 is essential in carcinogenesis. MLK4 regulates several physiological cellular processes, such as cell cycle, senescence, and apoptosis. Serine-threonine kinases, known as MLKs, are thought to control many intracellular signaling pathways. From

RCSB, PDB proteins were downloaded (PDB ID-4UYA). Further Glide XP (Extra Precision) docking protocol was followed for molecular docking. Glide XP docking is used to identify the best ligand orientation relative to a rigid protein receptor geometry. Three approaches to sampling ligand conformational and positional degrees of freedom are available. The techniques for flexible ligand docking using Glide XP are presented in this unit, with the option of ligand restrictions or molecular ligand similarity. Then these conformations can be ranked using a scoring function to achieve docking.

2.3. Ligand preparation

The selected ligand Quercetin was downloaded from PubChem and imported to the LigPrep module, which was used to generate different conformers from the input structure. OPLS_2005 force field[9] was used to optimize the structure. After minimizing the structure, the prepared ligand and protein were subjected to docking analysis.

2.4. Molecular docking studies

The molecular docking study analyzed Quercetin's binding affinity and inhibitory action against the target receptor. The study was carried out on Glide XP docking; the prepared ligand was docked with the target protein's active site.[10,11] The receptor grid generation panel generated the grid box with the X, Y, and Z coordinates. The highest-dock-score binding conformation between the receptor and the newly created molecule was evaluated, contrasted, and selected for further MD simulation study.

2.5. Molecular dynamics simulation

MD simulation of the docked complex was performed in the GROMACS server for 100 ns. Prodrg server[12] was utilized to generate the topology and coordinates of the ligands. In addition, the protein files were generated through Gromacs using the GROMOS96 43a1 force field and solvated by the SPC water model.[13] A cubic box was generated with the size of about 2.0 Å and by deleting the unwanted water molecule by neutralizing the system by adding ions. NPT and NVT were maintained at 300 K with 100 ps. The Berendsen method was utilized to regulate the temperature inside the system. The solvent molecules were loosened, and the solutes were constrained to their initial positions during the 5,000 steps that the two formed systems and were subjected to a force of 100 kcal/mol. And finally, MD was executed at the simulation period of 100 ns.[14]

2.6. Binding free energy calculation

MMGBSA (Molecular Mechanics Generalized Born Surface Area) approach was one of the most acceptable methods to calculate the binding energy of the docked complex.[15] MMGBSA.py script was utilized to calculate the binding energy by using the force field OPLS_2005; it was calculated by using the equation,

$$\Delta G(\text{bind}) = \Delta G(\text{complex}) - [\Delta G(\text{receptor}) + \Delta G(\text{ligand})$$

2.7. ADME analysis

The ADME parameter is one of the essential criteria to filter out the drug-likeness of the small molecules. This analysis was carried out using the Qikprop module.[16] A ligand's toxicity is vital

for acting as an effective drug in novel drug development, and Qikprop generates physically relevant descriptions.

2.8. Pharmacophore feature

Pharmacophore characteristics include hydrophobic centroids, aromatic rings, hydrogen bond acceptors or donors, cations, and anions. These pharmacophore sites could be on the ligand itself.[17]

3. Results and discussion

3.1. Molecular geometry analysis

In this study, the DFT/B3LYP method with a cc-pVTZ basis set was used to optimize the molecular structure of the title molecule.[18] The optimized molecular geometry's energy value was calculated as 1103.81 a.u. The optimized molecular structure of the Quercetin molecule is seen in Figure 1. Table 1 lists the molecule's computed structural parameters, including bond length, bond angle, and dihedral angle values. The Quercetin molecule has C1 point group symmetry in its molecular geometry.

The Quercetin molecule's vibrational modes are all IR and Raman active, indicating that it has a non-centrosymmetric structure.[19] The absence of negative vibrational wavenumbers implies that the optimal molecular structure of the Quercetin molecule is located at a local minimum on the potential energy surface.[20]

3.2. Vibrational spectral analysis

Quercetin molecule has 32 atoms and 90 normal modes of vibrations that all belong to the same symmetry species. Table 2 shows the vibrational frequencies, IR intensity, and Raman scattering activity of the most stable optimal structure of the Quercetin molecule. Figure 2 illustrates the theoretically generated infrared and Raman spectra of the molecule. The theoretically predicted vibrational wavenumbers were well associated with the available experimental vibrational

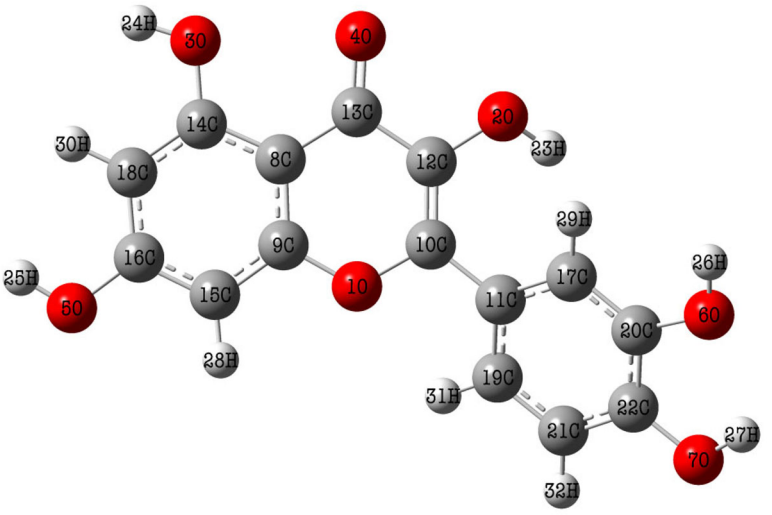

Figure 1. The optimized molecular structure of Quercetin molecule.

Table 1. The optimized structural parameters of the Quercetin molecule calculated by the DFT/B3LYP method with cc-pVTZ basis set.

Structural Parameters	cc-pVTZ	Structural Parameters	cc-pVTZ	Structural Parameters	cc-pVTZ
Bond length (Å)		Bond angle (°)		Bond angle (°)	
O1–C9	1.38	C16–O5–H25	112.28	C21–C19–H31	119.95
O1–C10	1.39	C20–O6–H26	113.12	O6–C20–C17	124.93
O2–C12	1.39	C22–O7–H27	109.77	O6–C20–C22	114.00
O–2–H23	0.97	C9–C8–C13	119.91	C17–C20–C22	121.05
O3–C14	1.37	C9–C8–C14	115.92	C19–C21–C22	120.11
O3–H24	0.97	C13–C8–C14	124.14	C19–C21–H32	121.37
O4–C13	1.24	O1–C9–C8	121.19	C22–C21–H32	118.51
O5–C16	1.38	O1–C9–C15	114.80	O7–C22–C20	120.35
O5–H25	0.97	C8–C9–C15	123.99	O7–C22–C21	120.22
O6–C20	1.39	O1–C10–C11	112.17	C20–C22–C21	119.41
O6–H26	0.97	O1–C10–C12	119.86	Dihedral angle (°)	
O7–C22	1.37	C11–C10–C12	127.93	C10–O1–C9–C8	−0.02
O7–H27	0.98	C10–C11–C17	120.84	C10–O1–C9–C15	−179.60
C8–C9	1.41	C10–C11–C19	120.38	C9–O1–C10–C11	178.05
C8–C13	1.47	C17–C11–C19	118.76	C9–O1–C10–C12	−3.46
C8–C14	1.42	O2–C12–C10	122.86	H23–O2–C12–C10	24.93
C9–C15	1.39	O2–C12–C13	113.92	H23–O2–C12–C13	−155.85
C10–C11	1.46	C10–C12–C13	123.20	H24–O3–C14–C8	179.66
C10–C12	1.36	O4–C13–C8	124.79	H24–O3–C14–C18	−0.29
C11–C17	1.41	O4–C13–C12	120.66	H25–O5–C16–C15	179.78
C11–C19	1.40	C8–C13–C12	114.53	H25–O5–C16–C18	−0.10
C12–C13	1.47	O3–C14–C8	118.24	H26–O6–C20–C17	2.23
C14–C18	1.39	O3–C14–C18	120.56	H26–O6–C20–C22	−177.33
C15–C16	1.39	C8–C14–C18	121.18	H27–O7–C22–C20	0.62
C15–H28	1.08	C9–C15–C16	117.96	H27–O7–C22–C21	−178.85
C16–C18	1.40	C9–C15–H28	120.82	C13–C8–C9–O1	1.77
C17–C20	1.38	C16–C15–H28	121.20	C13–C8–C9–C15	−178.68
C17–H29	1.08	O5–C16–C15	116.93	C14–C8–C9–O1	−179.32
C18–H30	1.08	O5–C16–C18	122.25	C14–C8–C9–C15	0.21
C19–C21	1.39	C15–C16–C18	120.81	C9–C8–C13–O4	179.21
C19–H31	1.08	C11–C17–C20	119.80	C9–C8–C13–C12	−0.18
C20–C22	1.40	C11–C17–H29	120.20	C14–C8–C13–O4	0.40
C21–C22	1.39	C20–C17–H29	119.88	C14–C8–C13–C12	−178.99
C21–H32	1.08	C14–C18–C16	120.10	C9–C8–C14–O3	179.84
C9–O1–C10	121.10	C14–C18–H30	119.64	O1–C9–C15–H28	−0.15
Bond angle (°)		C16–C18–H30	120.24	C8–C9–C15–C16	−0.07
C12–O2–H23	111.03	C11–C19–C21	120.84	C8–C9–C15–H28	−179.72
C14–O3–H24	111.37	C11–C19–H31	119.20	O1–C10–C11–C17	−149.26
Dihedral angle (°)		Dihedral angle (°)		Dihedral angle (°)	
O1–C10–C11–C19	29.42	O2–C12–C13–C8	177.45	C11–C17–C20–C22	0.17
C12–C10–C11–C17	32.40	C10–C12–C13–O4	177.23	H29–C17–C20–O6	−2.99
C12–C10–C11–C19	−148.90	C10–C12–C13–C8	−3.33	H29–C17–C20–C22	176.54
O1–C10–C12–O2	−175.64	O3–C14–C18–C16	−179.99	C11–C19–C21–C22	0.26
O1–C10–C12–C13	5.21	O3–C14–C18–H30	−0.05	C11–C19–C21–H32	−179.70
C11–C10–C12–O2	2.56	C8–C14–C18–C16	0.05	H31–C19–C21–C22	−179.50
C11–C10–C12–C13	−176.56	C8–C14–C1–H30	179.99	H31–C19–C21–H32	0.52
C10–C11–C17–C20	179.35	C9–C15–C16–O5	−179.98	O6–C20–C22–O7	−0.68
C10–C11–C17–H29	2.99	C9–C15–C16–C18	−0.08	O6–C20–C22–C21	178.79
C19–C11–C17–C20	0.64	H28–C15–C16–O5	−0.32	C17–C20–C22–O7	179.72
C19–C11–C17–H29	−175.71	H28–C15–C16–C18	179.56	C17–C20–C22–C21	−0.79
C10–C11–C19–C21	−179.58	O5–C16–C18–C14	179.98	C19–C21–C22–O7	−179.95
C10–C11–C19–H31	0.18	O5–C16–C18–H30	0.04	C19–C21–C22–C20	0.56
C17–C11–C19–C21	−0.86	C15–C16–C18–C14	0.09	H32–C21–C22–O7	0.01
C17–C11–C19–H31	178.90	C15–C16–C18–H30	−179.83	H32–C21–C22–C20	−179.46
O2–C12–C13–O4	−1.97	C11–C17–C20–O6	−179.36		

wavenumbers.[21–28] The vibrational wavenumbers of the molecule were assigned using the VEDA 4.0 software, which has been acknowledged as a helpful method for identifying vibrational frequencies by various studies.[29,30]

Table 2. The calculated vibrational frequencies (cm^{-1}), IR intensities (Km mol^{-1}), Raman scattering activity ($Å^4$ amu^{-1}), and vibrational assignments based on PED calculations for the Quercetin molecule.

ν_{cal}	[a]I IR	[b]I Raman	Assignment with PED%	ν_{cal}	[a]I IR	[b]I Raman	Assignment with PED%
3703	54.29	128.49	ν O–H (100)	1436	58.55	105.85	β O–H (45)
3672	54.26	241.48	ν O–H (98)	1348	115.25	199.50	β Φ C–H (28)
3644	26.14	264.74	ν O–H (98)	1310	61.78	23.60	β ϕ C–H (58)
3622	30.70	108.69	ν O–H (98)	1262	171.24	89.98	β ϕ C–H (52)
3619	122.76	206.47	ν O–H (98)	1224	278.28	52.86	β O–H (25)
3272	0.64	67.98	ν ϕ C–H (98)	1170	352.35	2.88	β ϕ C–H (28)
3254	2.33	96.95	ν Φ C–H (94)	1162	131.71	2.57	β O–H (33)
3236	4.71	94.69	ν Φ C–H (95)	1144	357.29	4.33	β ϕ C–H (55)
3203	3.17	26.28	ν Φ C–H (86)	1117	111.26	1.23	β O–H (36)
3181	18.29	149.18	ν ϕ C–H (78)	1070	117.94	6.29	ν ϕ C–O (38)
1690	236.36	48.46	ν ϕ C–C (48)	924	28.30	0.70	η Φ C–H (45)
1680	160.86	772.79	ν ϕ C–C (48)	801	52.06	4.87	η ϕ C–H (28)
1669	135.64	1341.7	ν ϕ C–C (46)	511	175.02	4.27	η Φ O–H (39)
1664	337.21	60.22	ν ϕ C–C (35)	426	89.87	0.69	η ϕ O–H (33)
1579	113.98	20.52	β Φ C–H (38)	399	163.75	7.60	η O–H (28)
1481	206.77	10.10	β ϕ C–H (38)	372	142.02	4.64	η O–H (29)

ν: stretching; β: in-plane bending; η: out of plane bending; ϕ: benzene ring 1 (left); Φ: benzene ring 2 (right); ν_{cal}: calculated vibrational frequency; [a]I IR: infrared spectra intensity; [b]I Raman: Raman scattering activities.

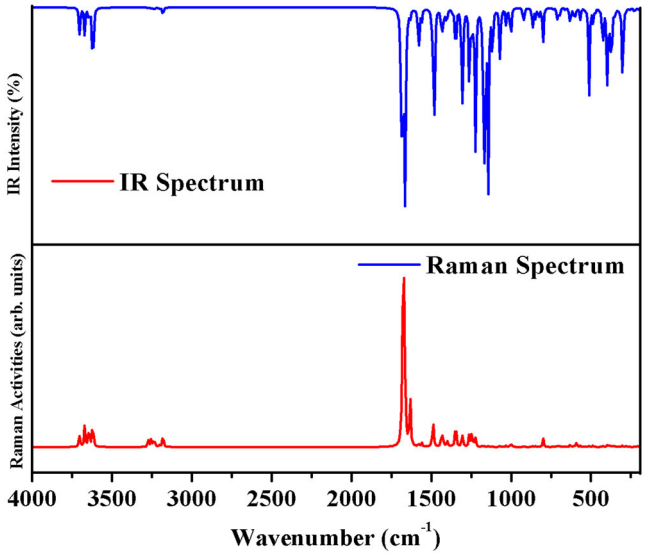

Figure 2. The simulated infrared and Raman spectra of Quercetin molecule.

3.3. Frontier molecular orbitals (FMOs) analysis

FMOs are typically used to define how a molecule interacts with other species.

FMOs are the highest occupied molecular orbital (HOMO) and the lowest unoccupied molecular orbital (LUMO). The HOMO energy indicates the capacity to give electrons, whereas the LUMO energy indicates the ability to transport electrons.[31] FMOs are essential in electric and optical characteristics, UV–Vis spectra, and quantum chemistry.[32] The HOMO–LUMO gap explains the molecule's kinetic stability and chemical reactivity, critical characteristics in defining its electronic properties. A soft molecule has a short HOMO–LUMO gap, limited kinetic stability, and high chemical reactivity. Figure 3 depicts the molecule's FMOs, and FMO's related molecular properties were calculated using Koopman's theorem, which is listed in Table 3.[33,34] In Figure 3, the positive phase is denoted by red, whereas the negative phase is depicted in green. As listed in Table 3.

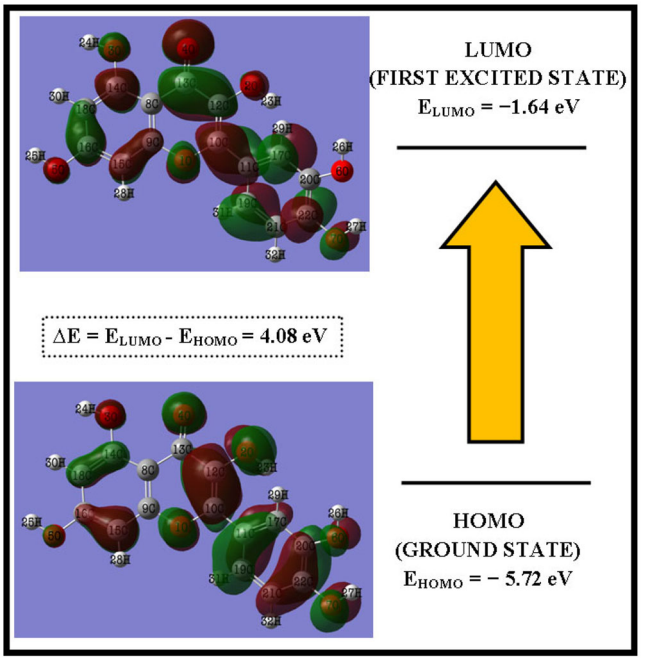

Figure 3. FMOs of Quercetin molecule.

Table 3. The calculated FMOs related molecular properties of the Quercetin molecule.

Molecular properties	Energy (eV)
E_{HOMO}	−5.72
E_{LUMO}	−1.64
Energy gap	4.08
Ionization energy (I)	5.72
Electron affinity (A)	1.64
Global hardness (η)	2.04
Global softness (S)	0.49
Chemical potential (μ)	−3.68
Electrophilicity index (ψ)	3.31

The calculated low energy gap value (4.08 eV) verifies the increased chemical reactivity of the Quercetin molecule. It explains the molecule's intramolecular charge transfer interaction, which determines the bioactivity of the molecule.[35,36] Ionization energy (I) is necessary to remove an electron from a filled orbital. Electron affinity (A) is the energy released when an electron is added to an empty orbital.

The higher ionization energy (5.72 eV) and low electron affinity (1.64 eV) imply that electrophilic and nucleophilic reactive sites are conceivable. The molecule's global hardness, $\eta = 2.04$ eV, global softness, $S = 0.49$ eV, chemical potential, $\mu = -3.68$ eV, and global electrophilicity index, $\psi = 3.31$ eV, were also estimated. The calculated hardness and softness values indicate that the molecule is stable. The molecule's anticipated chemical potential and electrophilicity index values support its chemical stability, comparable to that of a potent bioactive compound.[37–39]

3.4. UV-Visible spectral analysis

The TD-DFT/B3LYP method with a cc-pVTZ basis set was used to simulate the Quercetin molecule's UV-Visible spectra. A TD-DFT approach may investigate molecules' static and dynamic

characteristics in excited states.[40,41] The B3LYP method gives good results concerning the molecules' molecular geometry and physicochemical properties. Figure 4 shows the simulated UV-Visible spectra of the Quercetin molecule in gas and ethanol phases. The estimated absorption wavelengths (λ), excitation energy (E), and oscillator strength (f) for the gas phase and ethanol phase are listed in Table 4. As indicated in Figure 4, the first peak for the solvent was obtained at around 309 nm, whereas the matching peak for the gas phase was obtained at around 293 nm. The second peak was most substantial in the gas phase and solvent, about 331 and 346 nm, respectively. Figure 4 shows a considerable bathochromic shift (redshift) of absorption maxima in the solvent phase compared to the gas phase. Because excited states are more polar than ground states, the dipole interaction between solvent molecules and the solute decreases the energy of the excited state more than the ground state.[42,43]

3.5. MEP surface analysis

MEP surface analysis visualizes a molecule's chemically active areas, which aids in understanding molecular reactivity, electrophilic reactions, substituent effects, and intramolecular interactions.[43] The MEP surface of the Quercetin molecule is shown in Figure 5. Electron-rich, somewhat electron-rich, slightly electron-deficient, and electron-deficient areas are represented on the MEP surface by red, yellow, light blue, and blue, respectively. Because of the lone pair of oxygen atoms, the areas surrounding the oxygen atoms were electron-rich (red). All hydrogen atoms had a somewhat electron-deficient (light blue) region in the molecule. The area surrounding the hydrogen atoms H25 and H26 was discovered to be electron deficient (blue). The neutral electrostatic potential envelopes (green) were projected over the molecule. From the MEP analysis, the hydrogen atom H26 and the oxygen atom O6 are possible electrophilic and nucleophilic attack sites.

3.6. Mulliken atomic charge distribution analysis

The Mulliken atomic charge distribution affects the dipole moment, polarizability, electronic structure, vibrational modes, electrostatic potential model outside the molecular surface, and electronegativity equalization process of a molecule.[44] The estimated Mulliken atomic charge

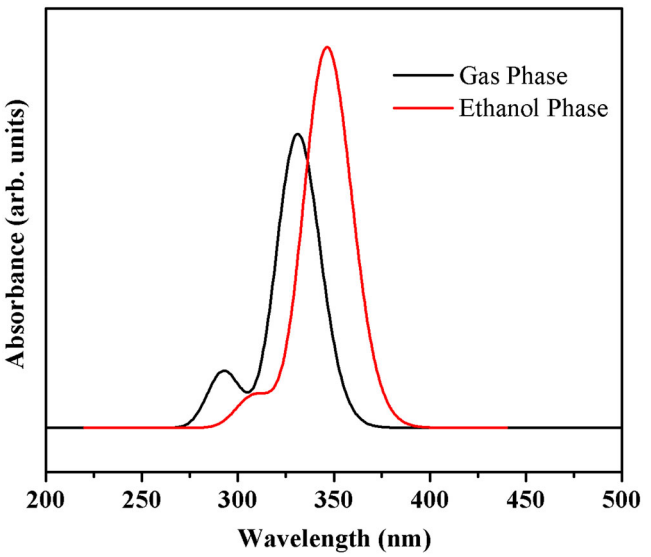

Figure 4. The simulated UV-Visible spectra of Quercetin molecule in gas phase and ethanol phase.

Table 4. The calculated absorption wavelength λ (nm), excitation energy values E (eV), oscillator strength (f), and orbital contributions for Quercetin molecule with its assignments.

Solvents	λ (nm)	E (eV)	f	Orbital contributions	Assignments
Gas	293	4.23	0.0716	H-2→L (85%)	$\pi\rightarrow\pi^*$
	331	3.75	0.3702	H→L (91%)	$n\rightarrow\pi^*$
Ethanol	309	4.01	0.0413	H-1→L (93%)	$\pi\rightarrow\pi^*$
	346	3.59	0.3755	H→L (76%), H-3 →L (18%)	$n\rightarrow\pi^*$

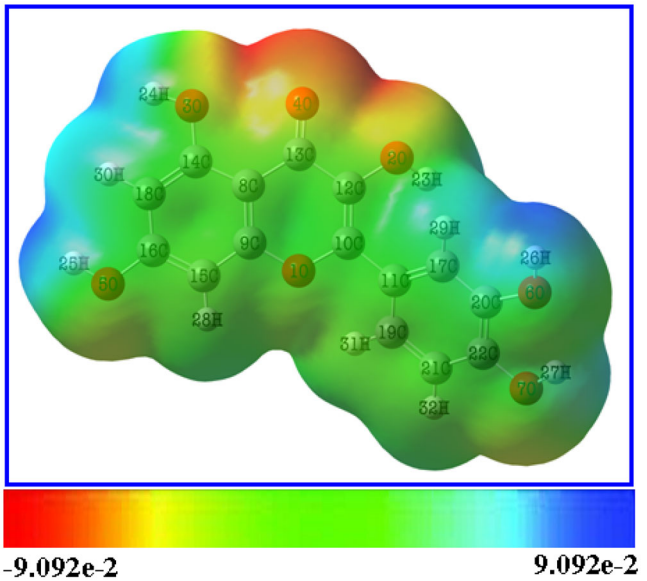

Figure 5. MEP surface of the Quercetin molecule.

Table 5. The calculated Mulliken atomic charge distribution of the Quercetin molecule.

Atom	Charge value	Atom	Charge value	Atom	Charge value	Atom	Charge value
O1	−0.596	C9	0.218	C17	−0.171	H25	0.377
O2	−0.591	C10	0.256	C18	−0.145	H26	0.390
O3	−0.567	C11	0.023	C19	−0.121	H27	0.401
O4	−0.392	C12	0.192	C20	0.232	H28	0.164
O5	−0.620	C13	0.259	C21	−0.125	H29	0.165
O6	−0.657	C14	0.198	C22	0.279	H30	0.116
O7	−0.619	C15	−0.109	H23	0.369	H31	0.158
C8	0.129	C16	0.263	H24	0.372	H32	0.153

distribution values for the Quercetin molecule are shown in Table 5. According to Table 5, the hydrogen atom H26 (0.390) and the oxygen atom O6 (0.657) have higher positive and negative charge values, respectively. The carbon atoms have a considerable negative charge value, which confirms electron delocalization inside the molecule. The Mulliken atomic charge distribution of the molecule reveals that all hydrogen atoms have positive charge values, whereas all oxygen atoms have negative charge values. On the other hand, carbon atoms have both positive and negative charge values. Therefore, their substituents outnumber carbon atoms. H26 has a higher positive charge value (0.390) than other hydrogen atoms due to the electronegative oxygen atom O6 attached to it. The atomic charge analysis performed by Mulliken reveals that the hydrogen atom H26 and the oxygen atom O6 are possible electrophilic and nucleophilic attack sites, respectively.

As a consequence of this conclusion, the MEP surface analysis is verified.

Table 6. Docking analysis of Quercetin with the target protein (PDB ID: 4UYA).

PDB ID	Compound	Docking score (Kcal/Mol)	Interacting residues	Binding free energy (Kcal/Mol)
4UYA	QUERCETIN	−10.239	Glu_201, Ala_203 (HB)	−59.724

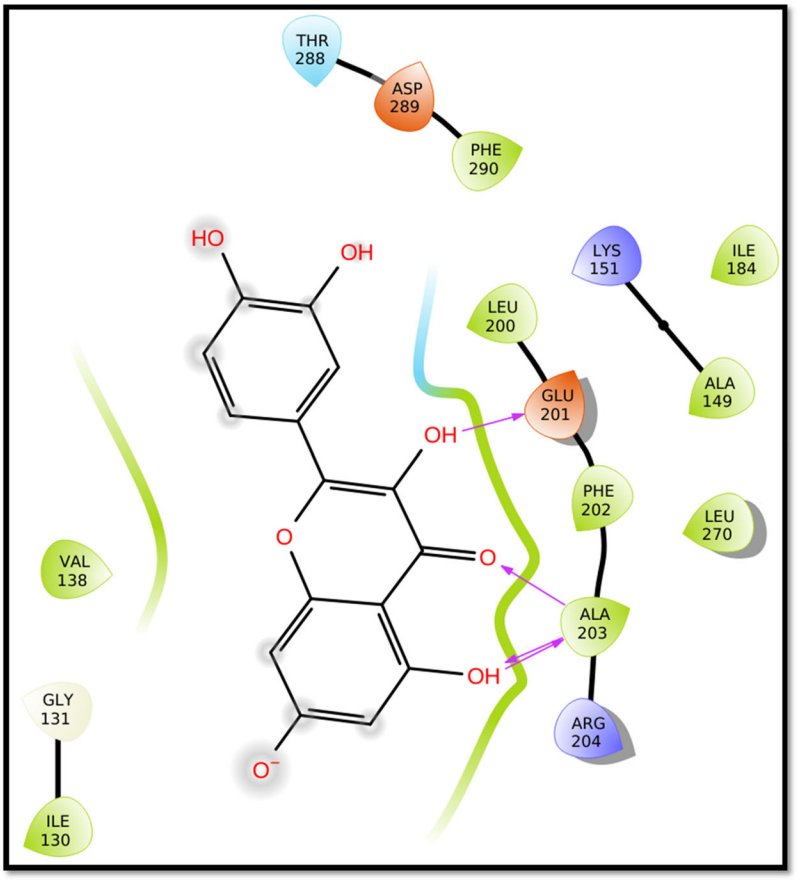

Figure 6. Docking analysis of Quercetin with the target protein (PDB ID: 4UYA).

3.7. Molecular docking and binding free energy

The docked complex 4UYA_Quercetin showed the highest docking score of about −10.239 Kcal/Mol, and hydrogen bond interaction occurred with the residues Glu_201, Ala_203. These residues depicted the hydrogen bond interactions essential for biological activity. The docked complex also showed better binding energy of about −59.724 Kcal/Mol; the negative implies the best binding affinity, and the findings were tabulated in Table 6 and displayed in Figure 6. To ensure the stability of the complex, MD was performed for 100 ns.

3.8. Molecular dynamics simulation

The stability of the docked complex was evaluated through Root Mean Square Deviation (RMSD), Root Mean Square Fluctuation (RMSF), and Hydrogen bond. After the 100 ns of simulation, RMSD, RMSF, and hydrogen bonds were analyzed through Xmgrace. RMSD plot showed the slightest deviation in the initial period and maintained better stability throughout the simulation. RMSF plot

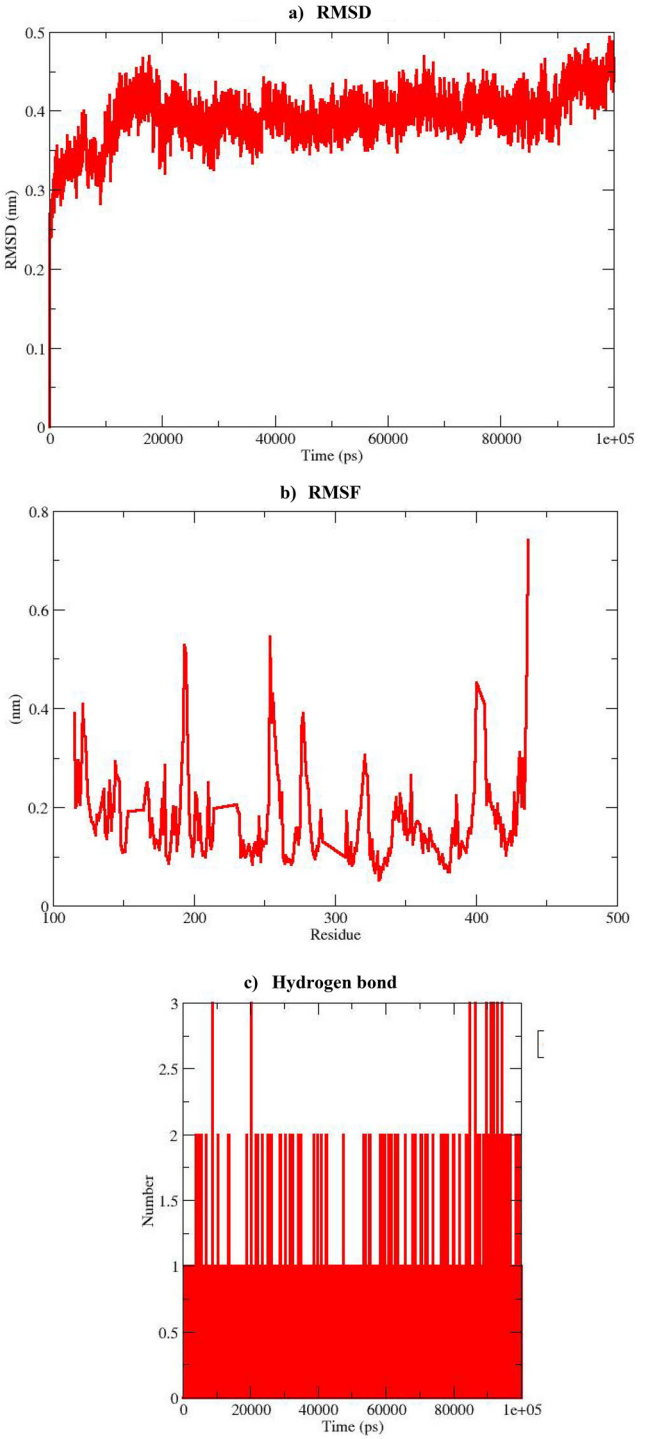

Figure 7. Molecular dynamics simulation of the complex 4UYA_Quercetin.

Table 7. ADME properties of Quercetin.

Compound	Mol. Wt	HB donor	HB acceptor	HOA (%)	Rule of five	QPPCaco	QPlogBB	QPlogPo/W
Quercetin	302.24	4.00	5.25	52.98	0	21.95	−2.254	0.347

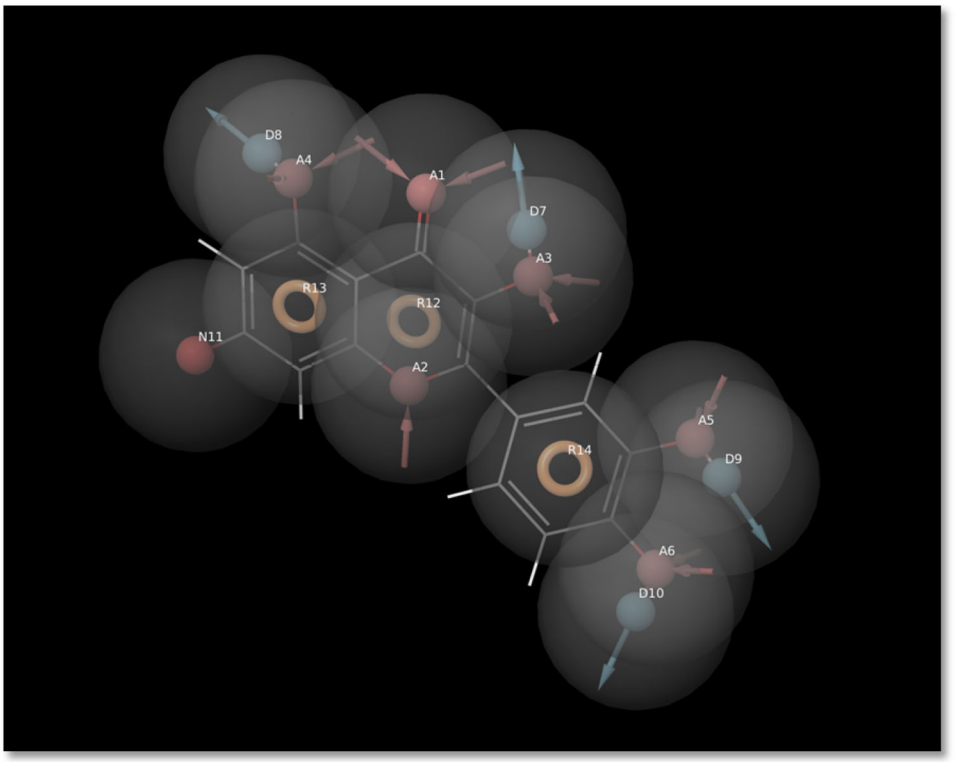

Figure 8. Pharmacophore features of Quercetin.

elucidated the fluctuation rate. A modest fluctuation was noted, not affecting the complex's stability. The hydrogen bond was noted as 3, illustrated in Figure 7, and the results concluded that the complex showed a better docking score, binding affinity, and stability.

3.9. ADME prediction

Pharmacokinetics, a branch of biology, describes the total deposition of a drug as a result of the processes of absorption, distribution, metabolism, and excretion. A promising drug's potential could be spoiled by the limiting characteristics of absorption, distribution, metabolism, excretion, and toxicity (ADMET). Additionally, the pharmacokinetic qualities of the medicine, which make it exceedingly expensive, are seen to be the main disadvantage of drug development in clinical trials. Table 7 shows the pharmacokinetic properties of the compound. The results concluded that Quercetin obeyed Lipinski's Rule of five by having a molecular weight of about 302.24, the Hydrogen Bond donor and acceptor were *n* the acceptable range (4.00 and 5.25), and the log *p*-value was also in the acceptable range.

3.10. Pharmacophore feature

Pharmacophore features are used to determine the small molecule's chemical features and generate pharmacophore models automatically based on the overlap of these common characteristic

structures. Quercetin has the following pharmacophore features: Donor, acceptor, and Ring, which are displayed in Figure 8.

4. Conclusion

In the present investigation, the molecular structure of the Quercetin molecule was optimized. The vibrational wavenumbers of the molecule were also calculated, which correlated well with the reported experimental values. In FMOs analysis, the obtained lower energy gap value indicates the possible biomedical actions of the Quercetin molecule. MEP surface and Mulliken atomic charge distribution analyses reveal that the hydrogen atom H26 and the oxygen atom O6 are possible electrophilic and nucleophilic attack sites, respectively. The inhibitory efficacy of the Quercetin molecule was examined against colon cancer-associated targeted protein through molecular docking and dynamics studies. The docked complex showed better binding affinity and structural stability with the most potent hydrogen bond interactions. The interacting residues, such as Glu_201 and Ala_203, had hydrogen bond interactions with Quercetin; RMSD and RMSF analysis revealed the stability of the docked complex with lesser deviation and fluctuations. Therefore, the present investigation concludes that the Quercetin molecule can act as a potent inhibitor for treating colon cancer.

Acknowledgments

Author J. Abraham Hudson Mark thankfully acknowledges the Department of Bioinformatics, Alagappa University, for providing Computational Laboratory facilities to carry out Bioinformatics studies.

Disclosure statement

No potential conflict of interest was reported by the author(s).

References

1. V. Asma, S. Zahra, M. Ahmad, F. Farzaneh, T. Mona, G. Younes, A. Maryam, S. Alimohammad, H. Sarah, M. Sanaz, et al., "Quercetin and Cancer: New Insights into Its Therapeutic Effects on Ovarian Cancer Cells," *Cell & Bioscience* 10, no. 1 (2020): 32.
2. Si-Min Tang, Xue-Ting Deng, Jian Zhou, Quan-Peng Li, Xian-Xiu Ge, and Lin Miao, "Pharmacological Basis and New Insights of Quercetin Action in Respect to Its Anticancer Effects," *Biomedicine & Pharmacotherapy* 121 (2020): 109604.
3. S. Srivastava, R. R. Somasagara, M. Hegde, M. Nishana, S. Tadi, M. Srivastava, B. Choudhary, and S. C. Raghavan, "Quercetin, a Natural Flavonoid Interacts with DNA, Arrests Cell Cycle and Causes Tumor Regression by Activating Mitochondrial Pathway of Apoptosis," *Scientific Reports* 6 (2016): 24049.
4. Susan Abraham, C. Muthu, S. Christian Prasana, J. Armakovic, S. Armakovic, S. J. Fathima Rizwana, B. Ben Geoffrey, Antony Host, and R. David, "Computational Evaluation of the Reactivity and Pharmaceutical Potential of an Organic Amine: A DFT, Molecular Dynamics Simulations and Molecular Docking Approach," *Spectrochimica Acta Part A: Molecular and Biomolecular Spectroscopy* 222 (2019): 117188.
5. M. Martini, M. Russo, S. Lamba, E. Vitiello, E. H. Crowley, F. Sassi, D. Romanelli, M. Frattini, A. Marchetti, and A. Bardelli, "Mixed Lineage Kinase MLK4 Is Activated in Colorectal Cancers Where It Synergistically Cooperates with Activated RAS Signaling in Driving Tumorigenesis," *Cancer Research* 73, no. 6 (2013): 1912–21.
6. Frisch, M.J., Trucks, G.W., Schlegel, H.B., Scuseria, G.E., Robb, M.A., Cheeseman, J.R., Scalmani, G., Barone, V., Mennucci, B., Petersson, G.A., Nakatsuji, H., Caricato, M., Li, X., Hratchian, H. P., Izmaylov, A. F., Bloino, J., Zheng, G., Sonnenberg, J. L., M. Hada, … D. J. Fox. (2013). *Gaussian 09, revision A.1.* Gaussian Inc. Wallingford.
7. S. Seshadri, S. Gunasekaran, S. Muthu, S. Kumaresan, and R. Arunbalaji, "Vibrational Spectroscopy Investigation Using *Ab Initio* and Density Functional Theory on Flucytosine," *Journal of Raman Spectroscopy* 38, no. 11 (2007): 1523–31.

8. P. Sangavi and K. Langeswaran, "Anti-Tumorigenic Efficacy of Tangeretin in Liver Cancer-An in- Silico Approach," *Current Computer-Aided Drug Design* 17, no. 3 (2021): 337–43.
9. P. Sangavi and K. Langeswaran, "Identification of Potential Elephantiasis Inhibitors against UDP-Galactopyranose Mutase (UGM) Using Virtual Screening and Molecular Docking," *Current Enzyme Inhibition* 17, no. 1 (2021): 57–70.
10. K. Choubey Sanjay and J. Jeyakanthan, "A Mechanistic Approach to Explore Novel HDAC1 Inhibitor Using Pharmacophore Modeling, 3D-QSAR Analysis, Molecular Docking, Density Functional and Molecular Dynamics Simulation Study," *Journal of Molecular Graphics & Modelling* 70 (2016): 54–69.
11. M. Erol, I. Celik, E. Uzunhisarcikli, and G. Kuyucuklu, "Synthesis, Molecular Docking, and DFT Studies of Some New 2,5-Disubstituted Benzoxazoles as Potential Antimicrobial and Cytotoxic Agents," *Polycyclic Aromatic Compounds* 42, no. 4 (2022): 1679–96.
12. A. W. Schüttelkopf and D. M. F. van Aalten, "PRODRG: A Tool for High-Throughput Crystallography of Protein-Ligand Complexes," *Acta Crystallographica. Section D, Biological Crystallography* 60, no. Pt 8 (2004): 1355–63.
13. P. Sangavi, R. Rajapriya, Firthous Sannathul, K. Langeswaran, and S. Gowtham Kumar, "Identification of Bioactive Compounds and Potential Inhibitors for Breast Cancer from *Musa sapientum* Peel – An *In Vitro* and *In Silico* Approach," *Research Journal of Biotechnology* 16, no. 7 (2021): 180–96.
14. Stève-Jonathan Koyambo-Konzapa, R. Premkumar, Ramlina Vamhindi Berthelot Saïd Duvalier, Mbesse Kongbonga Gilbert Yvon, Mama Nsangou, and A. Milton Franklin Benial, "Electronic, Spectroscopic, Molecular Docking and Molecular Dynamics Studies of Neutral and Zwitterionic Forms of 3,4-Dihydroxy-L-Phenylalanine: A Novel Lung Cancer Drug," *Journal of Molecular Structure* 1260 (2022): 132844.
15. Chirasmita Nayak, and Sanjeev Kumar Singh, "*In Silico* Identification of Natural Product Inhibitors against Octamer-Binding Transcription Factor 4 (Oct4) to Impede the Mechanism of Glioma Stem Cells," *PLOS One* 16, no. 10 (2021): e0255803.
16. Schrödinger Release 2020–2. *QikProp* (New York, NY: Schrödinger, LLC, 2020).
17. R. Anitha, R. Sangeetha, E. Arockia Jeya Yasmi Prabha, J. Sangavi, and K. Langeswaran, "Synthesis, Crystallization, XRD, Hirshfeld Surface, Vibrational Spectra, and Quantum Chemical Studies and Computational Investigation of Caffeinium Bisulfate: A New Noncentrosymmetric Form," *Journal of Biomolecular Structure and Dynamics* (2021): 1–18.
18. T. Valarmathi, R. Premkumar, and A. Milton Franklin Benial, "Spectroscopic and Molecular Docking Studies on 1-Hydroxyanthraquinone: A Potent Ovarian Cancer Drug," *Journal of Molecular Structure* 1213 (2020): 128163.
19. A. Parameswari, S. Premkumar, R. Premkumar, and A. Milton Franklin Benial, "Surface Enhanced Raman Spectroscopy and Quantum Chemical Studies on Glycine Single Crystal," *Journal of Molecular Structure* 1116 (2016): 180–7.
20. T. Valarmathi, R. Premkumar, and A. Milton Franklin Benial, "Quantum Chemical and Molecular Docking Studies on 1,4-Bis(Methylamino)Anthraquinone: A DFT Approach," AIP Conference Proceedings, vol. 2270 (2020), 040001.
21. A. I. Almansour, N. Arumugam, S. M. Soliman, B. S. Krishnamoorthy, J. F. Halet, R. V. Priya, J. Suresh, D. M. Al-Thamili, F. A. Al-Aizari, and R. S. Kumar, "Stereo Selective Synthesis, Structure and DFT Studies on Fluoro- and Nitro-Substituted Spirooxindole-Pyrrolidine Heterocyclic Hybrids," *Journal of Molecular Structure* 1237 (2021): 130396.
22. J. F. Areans, I. Lopez, M. S. Wooley, J. C. Otero, and J. I. Marcos, "Vibrational spectrum and internal rotation in 2-methylpyrazine," *Journal of the Chemical Society, Faraday Transactions II* 84 (1988): 53.
23. L. J. Bellamy, *The Infra-Red Spectra of Complex Molecules* (New York, NY: John Wiley and Sons, Inc., 1975).
24. M. Karabacak, D. Karagoz, and M. Kurt, "Experimantal (FT-IR and FT-Raman Spectra) and Theoretical (*Ab Initio* HF and DFT) Study of 2-Chloro-5-Methylaniline," *Journal of Molecular Structure* 892, no. 1–3 (2008): 25–31.
25. R. Mohamed Asath, R. Premkumar, T. Mathavan, and A. Milton Franklin Benial, "Structural, Spectroscopic and Molecular Docking Studies on 2-Amino-3-Chloro-5-Trifluoromethyl Pyridine: A Potential Bioactive Agent," *Spectrochimica Acta. Part A, Molecular and Biomolecular Spectroscopy* 175 (2017): 51–60.
26. G. Socrates, *Infrared and Raman Characteristic Group Frequencies*, 3rd ed. (New York, NY: Wiley, 2001).
27. G. Varsanyi, *Assignments for Vibrational Spectra of Seven Hundred Benzene Derivatives*, vol. I (London: Adam Hilger, 1974).
28. Zhixu Zhou, Ye Liu, Qian Ren, Dehou Yu, and Hong Guang Lu, "Synthesis, Crystal Structure and DFT Study of a Novel Compound *N*-(4-(2,4-Dimorpholinopyrido[2,3-*d*]Pyrimidin-6-yl)Phenyl)Pyrrolidine-1-Carboxamide," *Journal of Molecular Structure* 1235 (2021): 130261.
29. R. Premkumar, Shamima Hussain, Stève-Jonathan Koyambo-Konzapa, Naidu Dhanpal Jayram, M. R. Meera, T. Mathavan, and A. Milton Franklin Benial, "SERS and DFT Studies of *2-(Trichloroacetyl)Pyrrole*

Chemisorbed on the Surface of Silver and Gold Coated Thin Films: In Perspective of Biosensor Applications," *Journal of Molecular Recognition* 34, no. 11 (2021): e2921.
30. R. Premkumar, Shamima. Hussain, T. Mathavan, K. Anitha, and A. Milton Franklin Benial, "Surface-Enhanced Raman Scattering and Quantum Chemical Studies of 2-Trifluoroacetylpyrrole Chemisorbed on Colloidal Silver and Gold Nanoparticles: A Comparative Study," *Journal of Molecular Liquids* 290 (2019): 111209.
31. S. J. Koyambo-Konzapa, G. Y. Mbesse Kongbonga, R. Premkumar, B. S. Duvalier Ramlina Vamhindi, M. Nsangou, and A. Milton Franklin Benial, "Spectroscopic, Quantum Chemical, Molecular Docking and Molecular Dynamics Investigations of Hydroxylic Indole-3-Pyruvic Acid: A Potent Candidate for Nonlinear Optical Applications and Alzheimer's Drug," *Journal of Biomolecular Structure and Dynamics* (2021): 1–14.
32. B. Babu, J. Chandrasekaran, B. Mohanbabu, Yoshitaka. Matsushita, and M. Saravanakumar, "Growth, Physicochemical and Quantum Chemical Investigations on 2-Amino 5-Chloropyridinium 4-Carboxybutanoate-an Organic Crystal for Biological and Optoelectronic Device Applications," *RSC Advances* 6, no. 112 (2016): 110884–97.
33. R. Mohamed Asath, R. Premkumar, T. Mathavan, and A. Milton Franklin Benial, "Spectroscopic and Molecular Docking Studies on *N*,*N*-di-Tert-Butoxycarbonyl (Boc)-2-Amino Pyridine: A Potential Bioactive Agent for Lung Cancer Treatment," *Journal of Molecular Structure* 1143 (2017): 415–23.
34. S. Muthu and E. Isac Paulraj, "Molecular Structure, Vibrational Spectra, First Order Hyper Polarizability, NBO and HOMO–LUMO Analysis of 4-Amino-3(4-Chlorophenyl) Butanoic Acid," *Solid State Sciences* 14, no. 4 (2012): 476–87.
35. S. Muthu, E. Elamurugu Porchelvi, M. Karabacak, A. M. Asiri, and S. S. Swathi, "Synthesis, Structure, Spectroscopic Studies (FT-IR, FT-Raman and UV), Normal Coordinate, NBO and NLO Analysis of Salicylaldehyde *p*-Chlorophenylthiosemicarbazone," *Journal of Molecular Structure* 1081 (2015): 400–12.
36. R. Premkumar, H. Shamima, S. J. Koyambo-Konzapa, D. J. Naidu, T. Mathavan, and A. Milton Franklin Benial, "SERS and DFT Investigations of Methyl 4-Bromo-1*H*-Pyrrole-2-Carboxylate Adsorbed on Silver and Gold Substrates: In Perspective of Biosensor Applications," *Journal of Molecular Structure* 1236 (2021): 130272.
37. F. A. L. Porta, T. C. Ramalho, R. T. Santiago, M. V. J. Rocha, and E. F. F. Cunha, "Orbital Signatures as a Descriptor of Regioselectivity and Chemical Reactivity: The Role of the Frontier Orbitals on 1,3-Dipolar Cycloadditions," *The Journal of Physical Chemistry. A* 115, no. 5 (2011): 824–33.
38. E. P. Rocha, H. A. Rodrigues, E. F. F. Cunha, and T. C. Ramalho, "Probing Kinetic and Thermodynamic Parameters as Well as Solvent and Substituent Effects on Spectroscopic Probes of 2-Amino-1,4-Naphthoquinone Derivatives," *Computational and Theoretical Chemistry* 1096 (2016): 17–26.
39. R. R. Silva, T. C. Ramalho, J. M. Santos, and J. D. Figueroa-Villar, "On the Limits of Highest-Occupied Molecular Orbital Driven Reactions: The Frontier Effective-for-Reaction Molecular Orbital Concept," *The Journal of Physical Chemistry. A* 110, no. 3 (2006): 1031–40.
40. T. K. Kuruvilla, S. Muthu, J. C. Prasana, J. George, and S. Sevvanthi, "Spectroscopic (FT-IR, FT-Raman), Quantum Mechanical and Docking Studies on Methyl[(3*S*)-3-(Naphthalen-1-Yloxy)-3-(Thiophen-2-yl)Propyl]Amine," *Journal of Molecular Structure* 1175 (2019): 163–74.
41. S. Saravanan and V. Balachandran, "Quantum Mechanical Study and Spectroscopic (FT-IR, FT-Raman, UV–Visible) Study, Potential Energy Surface Scan, Fukui Function Analysis and HOMO–LUMO Analysis of 3-Tert-Butyl-4-Methoxyphenol by DFT Methods," *Spectrochimica Acta. Part A, Molecular and Biomolecular Spectroscopy* 130 (2014): 604–20.
42. M. Anuratha, A. Jawahar, M. Umadevi, V. G. Sathe, P. Vanelle, T. Terme, V. Meenakumari, and A. Milton Franklin Benial, "SERS Investigations of 2,3-Dibromo-1,4-Naphthoquinone on Silver," *Spectrochimica Acta. Part A, Molecular and Biomolecular Spectroscopy* 105 (2013): 218–22.
43. T. Valarmathi, R. Premkumar, M. R. Meera, and A. Milton Franklin Benial, "Spectroscopic, Quantum Chemical and Molecular Docking Studies on 1-Amino-5-Chloroanthraquinone: A Targeted Drug Therapy for Thyroid Cancer," *Spectrochimica Acta. Part A, Molecular and Biomolecular Spectroscopy* 255, no. 3 (2021): 119659.
44. G. Pandimeena, R. Premkumar, T. Mathavan, and A. Milton Franklin Benial, "Spectroscopic, Quantum Chemical and Molecular Docking Studies on Methyl 6-Aminopyridine-3-Carboxylate: A Potent Bioactive Agent for the Treatment of Sarcoidosis," *Journal of Molecular Structure* 1231 (2021): 129996.